

An efficient nonlocal treatment for 3D damage modeling based on the background mesh concept

H. Li, X. Pan, H. Yuan*

University of Wuppertal, Department of Mech. Engineering, Germany

* Email: h.yuan@uni-wuppertal.de

Keywords: Nonlocal damage model, averaging integration method, background mesh, finite element method, ductile damage

Abstract. Nonlocal damage models are introduced to overcome the strain localization and mesh dependence problem. However, the convergence and computational efficiency are a big issue, especially for 3D analysis. To construct an efficient treatment for nonlocal damage modeling, a new integration algorithm is proposed in analogy to meshless methods in the present paper. This algorithm is easy to be implemented into commercial software and can be directly extended for complex material models. An integration algorithm for 3D domains is implemented in the commercial software ABAQUS via UMAT. Crack propagation in cracked specimens under both tension and bending condition is investigated and confirms that with the new algorithm the strain localization is eliminated. 3D modeling of cracking reveals high efficiency in computations. Computational results agree reasonably with experiments.

1. Introduction

In order to eliminate the strain localization or the mesh dependence problem existing in the conventional theory when the strain-softening or damage solids are analyzed, an internal length scale is often introduced in different ways. Generally speaking, elimination of strain localization can be classified three sorts. The first one is the integration algorithm, the local value of the evaluation points are replaced by the integration ones in there adjoining domains in these models [1-2], whose sizes are dominated by the intrinsic material length. A common difficulty in these models is in implementation into a commercial FEM code, moreover, searching adjoining points is storage- and time-consuming. Another important kind of nonlocal models [3–6] is so-called gradient theories by taking gradients of porosity or strains of all orders for regulating strain distributions. In all these models, additional degrees of freedom and equations are needed, which increase the computational cost. Furthermore, solving high-order gradient equations could cause convergence problems. The last broad group can be identified as the micro-polar continuum model [7–9] which can eliminate the strain localization in shear softening cases by introducing the extra rotating terms, but this model cannot be used for the tensile softening, especially in analysis of mode I crack propagation this kind of models is still to be improved.

In the present work, a new integration algorithm is proposed to implement the regulation of damage variables in the domain characterized by the intrinsic material length, based on the background element concept of meshless methods. Using the algorithm gradients of strains or other variables can be evaluated efficiently and accurately, the strain gradient theory for damage or plasticity can be easily implemented into the conventional FEM code.

2. Nonlocal damage model with the strain gradient

Both Aifantis [10] and Gao et al. [11] assume that the flow stress depends on strain gradients, that is, the effective stress can be expressed as

$$\bar{\sigma} = \sigma_0 \bar{F}(\bar{\varepsilon}, \nabla \bar{\varepsilon}, \nabla^2 \bar{\varepsilon}, \dots), \quad (1)$$

where σ_0 is the reference stress from uniaxial tension tests. \bar{F} is a dimensionless function describing material flow after yielding. $\dot{\bar{\varepsilon}} = (2\dot{\varepsilon}_{ij}^p \dot{\varepsilon}_{ij}^p / 3)^{1/2}$ stands for the equivalent plastic strain rate. The total equivalent plastic strain is defined based on the integration of the rate, $\bar{\varepsilon} = \int \dot{\bar{\varepsilon}} dt$. If the gradients vanish, Eq. (1) is the known stress-strain relationship from the tensile tests. Chen and Yuan [12-13] assume simply that the actual flow stress which is related to the gradient of the equivalent plastic strain as

$$\bar{\sigma} = \sigma_0 \sqrt{F^2(\bar{\varepsilon}) + L_i \|\nabla \bar{\varepsilon}\|}. \quad (2)$$

The material length scale L_i has been introduced by Fleck and Hutchinson [14] to characterize effects of the material micro-structure. In this present paper, a damage model based the first-order of plastic strain gradient is introduced following the GTN model [15] as:

$$Y(\bar{\varepsilon}^p, \nabla \bar{\varepsilon}^p) = \sigma_0 \left(F(\varepsilon^p) + L_i^\alpha |\nabla \bar{\varepsilon}^p|^\alpha \right), \quad (3)$$

where α is to be fitted using the experiments. In the equation above Y denotes yield stress of the matrix. Then, the yield condition of the GTN model is given by

$$\Phi(\mathbf{\sigma}, \bar{\varepsilon}^p, f^*) = \left(\frac{q}{Y(\bar{\varepsilon}^p, \nabla \bar{\varepsilon}^p)} \right)^2 + 2q_1 f \cosh \left(\frac{3q_2 p}{2Y(\bar{\varepsilon}^p, \nabla \bar{\varepsilon}^p)} \right) - (1 + q_1^2 f^{*2}), \quad (4)$$

where the constants q_1 and q_2 were introduced by Tvergaard [16] to consider interactions of voids. $\mathbf{S} = p\mathbf{I} + \boldsymbol{\sigma}$ is the deviatoric part of the macroscopic Cauchy tensor $\boldsymbol{\sigma}$; $q = (3\mathbf{S}:\mathbf{S}/2)^{1/2}$ is the Mises stress; p is the hydrostatic pressure, and f^* is the function of the void volume fraction (VVF), depending on the porosity of material, f . To consider rapid expansion of voids beyond the critical porosity f_c , Tvergaard and Needleman introduced bi-linear extrapolation of the porosity, f^* is defined as

$$f^* = \begin{cases} f, & f \leq f_c \\ f_c + \kappa(f - f_c), & f_c < f < f_l \\ 1.0/q_1, & f > f_l \end{cases} \quad (5)$$

with $\kappa = 3$ as the acceleration factor reflects the acceleration of void growth after coalescence, f_l is the value of VVF when the material is fully damaged. The evolution equation for VVF consists of both void nucleation and growth,

$$\dot{f} = \dot{f}_{growth} + \dot{f}_{nucleation} = (1-f)\dot{\varepsilon}_{kk}^p + A\dot{\varepsilon}^p, \quad A = \frac{f_N}{s_N \sqrt{2\pi}} \exp \left[-\frac{1}{2} \left(\frac{\bar{\varepsilon}^p - \varepsilon_N}{s_N} \right)^2 \right], \quad (6)$$

where $\dot{\varepsilon}_{ij}^p$ is the plastic strain rate tensor in the updated Lagrange configuration. A strain controlled nucleation law is suggested by Chu and Needleman where the parameter A is chosen so that the nucleation strain follows a normal distribution with mean value ε_N and standard deviation s_N . f_N is the volume fraction of the nucleated voids, and voids are nucleated only in tension. In this work, the void nucleation is not considered and f_N is taken as 0. So that

$$\dot{f} = \dot{f}_{growth} = (1-f)\dot{\epsilon}_{kk}^p. \quad (7)$$

The plastic strains are derived from the yield potential, Φ ; the presence of the first invariant of the stress tensor in the yield condition results in plastic strains:

$$\dot{\epsilon}^p = \dot{\lambda} \left(-\frac{1}{3} \frac{\partial \Phi}{\partial p} \mathbf{I} + \frac{3}{2q} \frac{\partial \Phi}{\partial q} \mathbf{S} \right), \quad (8)$$

where $\dot{\lambda}$ is the nonnegative plastic multiplier. The evolution of equivalent plastic strain is assumed to be governed by the equivalent plastic work expression, i.e.,

$$(1-f)\sigma_y \dot{\epsilon}^p = \boldsymbol{\sigma} : \dot{\epsilon}^p. \quad (9)$$

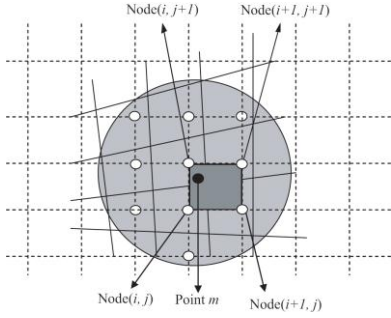


Figure 1. The sketch for the relationship between the evaluation point and the nodes on the background mesh in the case of 2D.

3. A new nonlocal approach

One big issue in gradient theory is in evaluating the gradient of strains or other field variables since the C_0 element formulation does not provide continuous distributions of them. Using C_1 element formulation causes difficulties in convergence [5,12]. The direct interpolation becomes unpractical for 3D computations. In Fig. 1, we show the topological relationship between the evaluation points and the nodes on the background mesh in the case of 2D. Because the element on the background mesh is a rectangular (in 2D) or a cuboid (in 3D), the nodes are very easy to be indexed. In 2D, suppose that the coordinate of left bottom node on this mesh is (x_0, y_0) , the element length and height are l_x and l_y , respectively. If the coordinate of the evaluation point m is (x, y) , we can easily get the index of a element which the evaluation point belongs to. The element index (i, j) can be expressed as following,

$$\begin{aligned} i &= \text{Integer}((x-x_0)/l_x + 1) \\ j &= \text{Integer}((y-y_0)/l_y + 1) \end{aligned} \quad (10)$$

so that we can get the node indices of this element: (i, j) , $(i+1, j)$, $(i+1, j+1)$ and $(i, j+1)$, which are the most closest nodes to this evaluation point. This algorithm can be extended to 3D directly, if the coordinates of the evaluation point m are (x, y, z) , then the index of associated element is given by,

$$\begin{aligned} i &= \text{Integer}((x-x_0)/l_x + 1) \\ j &= \text{Integer}((y-y_0)/l_y + 1) \\ k &= \text{Integer}((z-z_0)/l_z + 1) \end{aligned} \quad (11)$$

where (x_0, y_0, z_0) are the coordinates of left bottom node in the rear surface on the mesh and the element length, height and width are l_x , l_y and l_z , respectively, then the node indices of this element are: (i, j, k) , $(i+1, j, k)$, $(i+1, j+1, k)$, $(i, j+1, k)$, $(i, j, k+1)$, $(i+1, j, k+1)$, $(i+1, j+1, k+1)$ and $(i, j+1,$

$k+1$). Furthermore, we can get the nodes in the point influence domain, which is defined here as a circle (in 2D) or a ball (in 3D) centered at Point m . The radius of the circle/ball is the intrinsic material length L_i . At the end of every time step, the local incremental values at the evaluation points are known. In order to get the nonlocal value at Point m , the following procedure should be taken:

- (1) Mapping local incremental values to nodes of the background mesh, following the algorithm of meshless methods. For the evaluation point m , suppose the node number (on the background mesh) in its influence domain is m_1, m_2, \dots, m_I , respectively, where I is the total number. If the local incremental value is Δf_m , then Δf_m are mapped to these nodes, the values are $\Delta f_m W(r_m^{m_i})$, respectively, where $W(r_m^{m_i})$ is the weight function, and $r_m^{m_i}$ is the distance between the evaluation point and the node, which is usually defined as a compact function, such as

$$W(r) = \exp\left(-r/4\sqrt{l_x^2 + l_y^2}\right) \quad (2D), \quad W(r) = \exp\left(-r/4\sqrt{l_x^2 + l_y^2 + l_z^2}\right) \quad (3D). \quad (12)$$

After the loop for all the evaluation points (Gauss points in FEM), the mapped nodal incremental value at Node g is obtained, as

$$\Delta F_g = \frac{\sum_{j=1}^J W(r_j^{j_g}) \Delta f_j}{\sum_{j=1}^J W(r_j^{j_g})} \quad (13)$$

where J is the total number of the evaluation points whose influence domain covers the node g .

- (2) Generating the nonlocal value at the evaluation point. The nonlocal incremental value at evaluation point p can be expressed as

$$\bar{\Delta f}_p = \frac{\sum_{i=1}^I W(r_p^{p_i}) \Delta F_i}{\sum_{i=1}^I W(r_p^{p_i})}. \quad (14)$$

The averaging method presented above is based on the background element integration of meshless methods and can be applied to different material models. In GTN model, if we replace the incremental VVF with the nonlocal value, the nonlocal damage model with new integration algorithm is obtained. Furthermore, we can use this background mesh to compute the strain gradient terms in the strain gradient plasticity models. One just needs to replace f by strains.

4. Computational examples

4.1 Crack propagation simulation in a compact tension specimen.

A compact tension specimen (CT) with initial crack length of 25mm and width of 50mm is considered under plane strain condition. Due to the symmetry only the upper half of the specimen should be modeled. The German reactor pressure vessel steel, 20MnMoNi55, is assumed following the data in [17]. Three different meshes are considered to examine the mesh dependence, the lengths of the elements ahead of the crack tip are 0.1mm, 0.05mm and 0.025mm, respectively. The GTN model parameters are: $q_1=1.5$, $q_2=1.0$, the initial VVF $f_0=0.01$, the critical VVF $f_c=0.05$ and the final VVF $f_n=0.4$. The final contour of VVF distributions near the crack tip are shown in Fig. 2. In Fig. 2(a) are the results from the conventional GTN model, in which the obvious mesh dependence can be seen, and only one layer of elements is damaged, as the mesh becomes finer, the damage zone become thinner. In Fig. 2(b) are the results from the nonlocal GTN model by using the proposed integration algorithm, in which the intrinsic material length is taken as 0.2mm, the mesh dependence or strain localization problem is well eliminated. Fig. 3 shows the curves of loading vs. crack mouth

open displacement (CMOD). In Fig. 3(a) the loading depends on element size, while in Fig. 3(b) the dependence is eliminated.

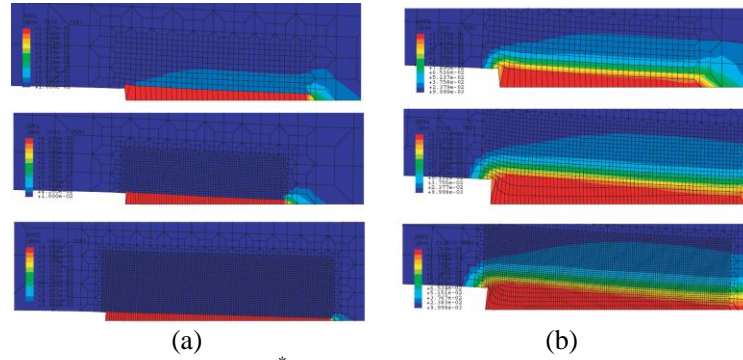


Figure 2. iso-contours of the porosity, f^* in CT specimens based on three different FEM meshes. (a) GTN model results. (b) Results from nonlocal model with $L_i=0.2\text{mm}$.

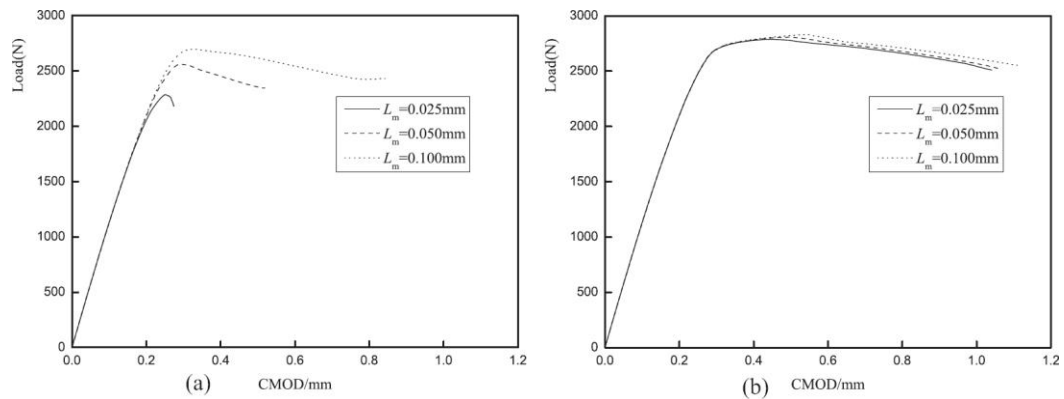


Figure 3. The loading vs. crack mouth open displacement (CMOD) of the CT specimen.

4.2 Crack propagation simulation in a bending specimen.

The plane stress bending specimen of 20MnMoNi55 is defined as following: $W=15.0\text{mm}$ and $a_0=7.0\text{mm}$. A small notch is set near the crack tip, and the radius of the notch is 0.5mm . The material model parameters as well as the FEM model structure are the same as those for the CT specimen in the previous section. Three different meshes have been considered. The minimal lengths of the elements are 0.20mm , 0.10mm and 0.05mm , respectively.

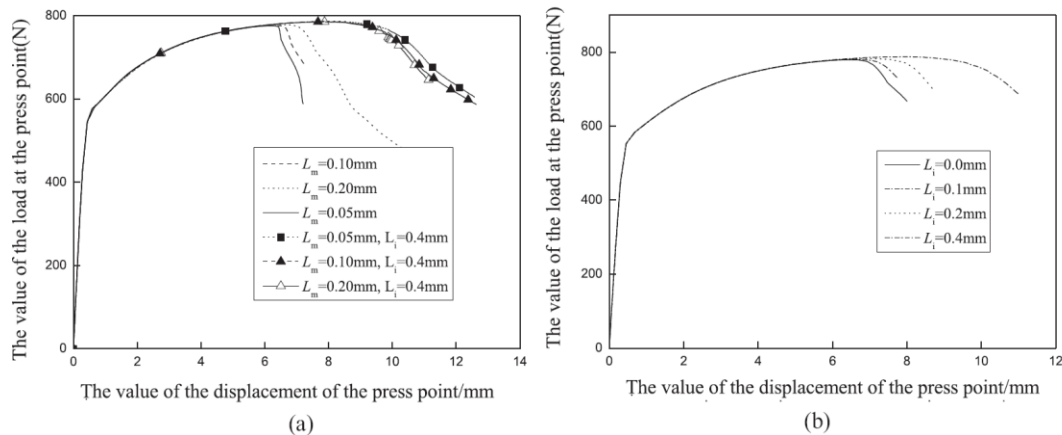


Figure 4. The load as a function of the load line displacement from three different meshes of the bending specimen are considered. (a) Results from the GTN model as well as the nonlocal model. (b) Effects of the intrinsic length L_i with $L_m=0.05\text{mm}$.

Figure 4 illustrates loading of the bending specimen as a function of the load line displacement from three different meshes. As known, the conventional GTN model shows strong dependence on the element size and the gradient regulator eliminates the mesh dependence displayed in Fig. 4(a), in which the intrinsic material length is set to 0.4mm. In Fig. 4(b) results of the nonlocal model with different intrinsic material lengths are summarized. Generally, the material length increases strength of material. Effects of the intrinsic length appear only before failure of the specimen.

3.3 Failure analysis in a 3D tensile bar

The geometry of the tensile bar is illustrated in Fig. 5(a), the initial gauge length is 32mm, the width is 5.7mm and the thickness is 5.55mm. For symmetry only one eighth of the tensile bar has to be modeled. The material property of 20MnMoNi55 is used. The initial mesh distribution is depicted in Fig. 5(b). To study the element dependence, three different meshes are considered with the minimal element lengths 0.15mm, 0.095mm and 0.05mm, respectively. The GTN model parameters for the CT specimen applied again: $q_1=1.5$, $q_2=1.0$, $f_0=0.01$, $f_c=0.02$ and $f_n=0.4$.

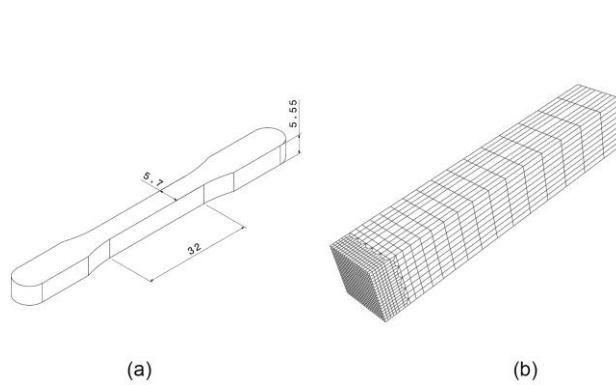


Figure 5. (a) Sketch map of the tensile bar and (b) the initial mesh distribution.

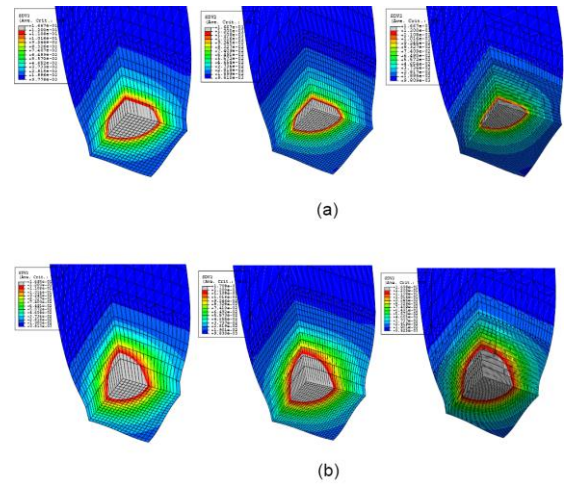


Figure 6. iso-contours of the porosity, f^* in the tensile bar based on three different meshes. (a) GTN model results. (b) Results from nonlocal model with $L_i=0.3$ mm.

The 3D VVF distribution contours at the end of the final fracture are plotted in Fig. 6. This kind of specimen is popular in powder metal industry. The stress field in such specimens is generally three-dimensional. Non-uniform distributions are obtained due to the complicated deformation pattern of the neck. As expected, the conventional GTN model reveals the strong element size dependence (Fig. 6(a)), the damage zone becomes thinner as the mesh becomes finer. Only one layer of elements is damaged in the computations. Nonlocal treatment in 3D specimen can be performed using the algorithm efficiently. In Fig. 6(b) the damage zone become independent of element size using the nonlocal model with the intrinsic material length equal to 0.3mm. The engineering stress-strain curves for three different mesh sizes are plotted in Fig. 7. In Fig. 7(a), the stress carrying capability is independent of FEM mesh, when stress-strain behavior is deformation hardened. The Effects of the mesh size becomes significant as soon as the ultimate stress is reached. The predicted material carrying capacity reduces with the smaller element size. The nonlocal model combined with the present computational algorithm provides an independent prediction of the material curve, as shown in Fig. 7(b). The intrinsic material length changes material behavior, especially before the final

failure. Fig. 8 reveals computational results with various intrinsic material lengths, whereas the element size in the damage zone is fixed. Obviously, the intrinsic length will only affect the final fracture strain, larger material length will arise the fracture strain. However, the computational prediction becomes unsystematic if the smallest element size is larger than the material length. The side necking seems less sensitive to the material length.

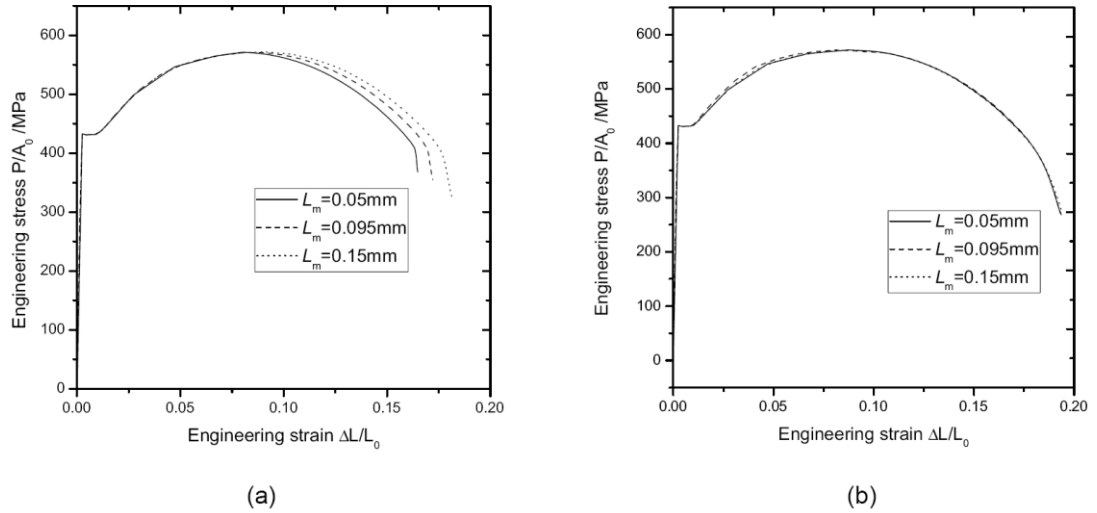


Figure 7. Effects of the element size to the engineering stress vs. engineering strain curves. (a) using the GNT model. (b) Prediction from the nonlocal model.

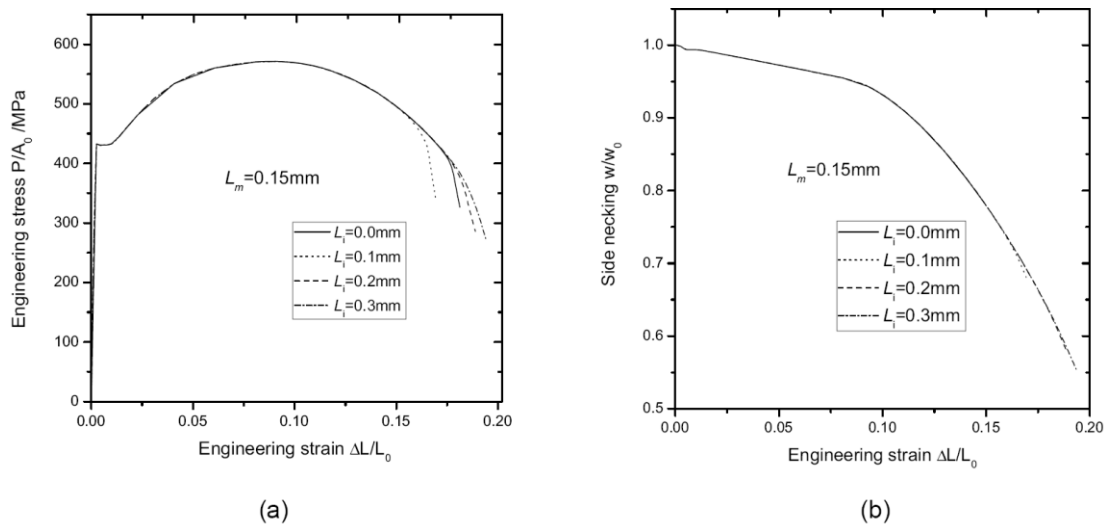


Figure 8. Effects of the intrinsic material length to the stress-strain curve using the mesh with $L_m=0.15$ mm. (a) The engineering stress vs. engineering strain. (b) Side necking vs. engineering strain.

Conclusions

In the present paper a new algorithm for nonlocal treatment in damage mechanics as well as gradient models has been introduced. Using the meshless method concept, the differentiation of the field variables can be performed based on the background mesh. A set of regular elements are introduced to bridge the evaluation point and the points used for the integration. The algorithm can be

implemented into the commercial FEM code easily. Both 2D and 3D computational examples confirm the present algorithm is accurate, reliable and efficient. The computational results agree with the known simulations.

The nonlocal model based on the first order of plastic strain gradient shows mesh-independent results in all studied cases. The strain localization can be well eliminated using the present model.

References

- [1] JB Leblond, G Perrin, J Devaux: *J. Appl. Mech.* Vol. 61 (1994), p. 236-241
- [2] V Tvergaard, A Needleman: *Int. J. Solids Struct.* Vol. 32 (1995), p. 1063-1077
- [3] S Ramasamy, N Aravas: *Comput. Method Appl. M.* Vol. 163 (1998), p. 33-53
- [4] RHJ Peerlings, R de Borst, W. A. M. Brekelmans and J. H. P. De Vree: *Int. J. Numer. Meth. Engng.* Vol. 39 (1996), p. 3391-3403
- [5] J Chen, H Yuan: *Int. J. Numer. Meth. Engng.* Vol. 18 (2002), p. 399-420
- [6] H Yuan, *Numerical Assessment of Cracks in Elastic-Plastic Materials*, Springer Verlag, Berlin (2002).
- [7] AC Eringen, DG Edelen: *Int. J. Engng Sci.* Vol. 10 (1972), p. 233-248
- [8] R de Borst: *Engineering Computations* Vol. 8 (1991), p. 317-332
- [9] W Huang, E Bauer: *Int. J. Numer. Anal. Meth. Geomech.* Vol. 27 (2003), p. 325-352
- [10] Aifantis EC: *Int. J. Plasticity*, Vol. 3 (1987), p. 211-247
- [11] H Gao, Y Huang, WD Nix, JW Hutchinson: *J. Mech. Phys. Solids* Vol. 47 (1999), p. 1239-1263.
- [12] H Yuan, J Chen: *Comp. Mater. Sci.* Vol. 19 (2000), p. 143-157
- [13] H Yuan, J Chen: *Int. J. Solids Struct.* Vol. 38 (2001), p. 8171-8187
- [14] NA Fleck, JW Hutchinson: *J. Mech. Phys. Solids* Vol. 41 (1993), p. 1825-1857
- [15] AL Gurson: *Journal of Engineering Materials and Technology* Vol. 99 (1977), p. 2-15
- [16] V Tvergaard, A Needleman: *Acta Metallurgica* Vol. 32 (1984), p. 157—169
- [17] X Pan, H Yuan: *Modelling Simulation Mater. Sci. Eng.* Vol. 46 (2009), p. 660—666